Bistatic synthetic aperture imaging of proud and buried targets from an AUV

Kevin D. LePage and Henrik Schmidt

Abstract— **The use of Autonomous Underwater Vehicles (AUV's) for the detection of buried mines is an area of current interest to the Mine Counter-Measures (MCM) community. AUV's offer the advantages of lower cost, stealth and potentially improved coverage rates over more traditional mine hunters. However, AUV's also come with their own set of challenges, including significant error in navigation, and communication difficulties with the mother platform and each other. In the case of bistatic detection scenarios, AUVs will therefore have difficulty knowing where exactly in space they are, and the trigger time of sources on other platforms, be they ships or other AUVs. However, the potential improvement in detection and coverage rates offered by bistatic sonar concepts makes resolution of these issues a high priority. In this paper the problems of inaccurate navigation and source timing information are addressed for the GOATS'98 data set. In this experiment, conducted off Marciana Marina during June 1998, a MIT AUV with a SACLANTCEN acoustic array and acquisition system was used together with a TOPAS parametric sonar to explore issues of buried target detection using AUVs. In this paper solutions to the navigation and timing problems are proposed which enable the effective use of bistatic Synthetic Aperture Sonar (SAS) concepts for the detection of buried objects in the mid frequency regime of 2-20 kHz.**

Keywords— **buried mines ∘ AUV ∘ synthetic aperture ∘ bistatic imaging**

I. Introduction

IN June of 1998, a joint MIT/SACLANTCEN experiment called GOATS'98 (Generic Oceanographic Array Technology) was conducted off Marciana Marina on the island of Elba in the Tyrrhenian Sea in very shallow water for the purpose of evaluating the detection of mine-like objects buried in the seafloor [1]. A MIT Odyssey II AUV equipped with a SACLANTCEN acoustic nose array and acquisition system was used to survey the scattering from a target field excited by the Centre's highly directional TOPAS parametric array at various grazing angles ranging from above to below critical angle. Subcritical detection of buried objects is an important goal of advanced mine hunting sonar concepts, but the extremely low ensonification levels on buried objects at incident angles below critical imply that significant array gains are required to make object detection feasible. The conventional approach to obtaining the required gain is to explore SAS concepts. The GOATS'98 data set, with inherently inaccurate navigation data from the Long BaseLine (LBL) navigation system, bistatic source-receiver geometries, and a lack of TOPAS trigger times due to communication limitations between the AUV and the TOPAS, places new demands on SAS concepts. In this paper these limitations are addressed and subcritical detection of buried objects on a bistatic synthetic aperture collected by an AUV in the 2 to 20 kHz frequency band is demonstrated.

K.D. LePage is with the SACLANT Undersea Research Centre, Viale San Bartolomeo 400, 19138 La Spezia, Italy. E-mail: lepage@saclantc.nato.int .

H. Schmidt is MIT Professor of Ocean Engineering, 77 Massachusetts Avenue, Cambridge, MA 02139. E-mail: henrik@keel.mit.edu .

II. Experimental Description

The experimental geometry of GOATS'98 is shown in Fig. 1, where the target field, consisting of three 1 m diameter water-filled steel spheres S1, S2 and S3, with center burial depths of 0, 0.5 and 1 m are shown being ensonified by a TOPAS source generating a highly directional beam in the secondary frequency band of 2 to 20 kHz. The depth of the water over the target field was 13.5 m. The TOPAS source itself was mounted on a 10 m tall tower which could be moved along a horizontal rail lying on the seafloor. The average depth of the TOPAS rail was 14.3 m. This tower and rail arrangement allowed the angle of incidence of the TOPAS beam on the seafloor above the flush buried sphere S2 to be adjusted between 16.2° and 34.6° [1]. This range of incident angles included the important subcritical grazing angles below 22.9°, as the bottom in the Marciana Marina area is sandy with an average near sediment-water interface sound speed of approximately 1650 m/s in the frequency band of interest[2].

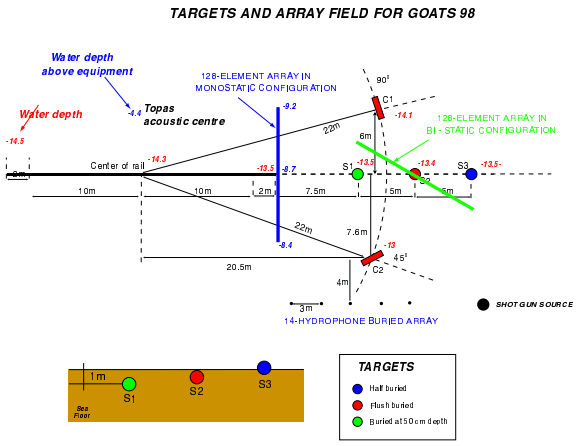

Fig. 1. The experimental configuration for GOATS 98 showing the 10 m tall TOPAS tower at a 10 m rail position which illuminates the target field of buried spheres. The TOPAS position for the data collected during experiment x9814501 is 5 m further to the left, from which point the flush buried sphere *S2* is ensonified below critical angle at an angle of 18.7°. The data analyzed for experiment x9814601 where collected when the source was 2.5 m further to the right, from which point S2 was ensonified at 24.4°

The MIT Odyssey II AUV was programmed to swim

missions over the target field while various targets were directly ensonified by the TOPAS at various grazing angles. The vehicle transited the target field at an average height of approximately 7.5 m and at an average speed of approximately 1 m/s. In this paper we confine our attention to the data set x9814501, where the TOPAS tower was at a 5 m position along the rail and was aimed at the proud target S3 at a 16.2° grazing angle, and to the data set x9814601, where the TOPAS tower was at a 12.5 m position along the rail and was aimed at the flush buried target S2 at a 24.4° grazing angle. In the first experiment, the TOPAS tower was 34.5 m from the proud sphere, and with it's 4° vertical and 9° horizontal beampattern [3] it ensonified a patch centered on S3 which extended roughly 9.2 m in range and 5.5 m laterally. In this geometry the flush buried sphere S2 was ensonified at a grazing angle of 18.7° and because of the size of the ensonified patch it received adequate power to be detected. However, because S2 was illuminated at an angle roughly 4° below the critical angle, the scattered returns measured from this target are significantly smaller than those measured from the proud sphere S3. In the second experiment, both S2 and the deeply buried sphere S1 were ensonified above the critical angle, making their detection significantly easier.

Since the Odyssey AUV was operating without time synchronization with the TOPAS system, it was decided to trigger the TOPAS off the AUV's navigation interrogation pulse. Every ten seconds, the vehicle would interrogate the LBL system with a 8 kHz ping. The LBL network, which consisted of 6 buoys with transponders operating in the 8 to 10.5 kHz range, would then respond and the vehicle computer would use the round trip travel times to update it's navigational estimate. The TOPAS would also detect the AUV's interrogating pulse, and after waiting 2 s for the reverberation from the pingers to die out, would commence to broadcast 8 kHz Ricker waveforms at a source level of 201 dB re μPa every 300 ms. At the same time the interrogating pulse was sent, the acquisition system on the AUV would begin to collect a 10 s long data file off an eight element horizontal line array of hydrophones which was deployed off the nose of the vehicle as illustrated in Fig. 2. This array was designed to receive the scattered field caused by the illumination of the target field by the TOPAS, and has a design frequency of 7.5 kHz and a sample rate of 50 kHz. Since the total field interrogated by the AUV nose array had a large dynamic range, the acquisition system, which was only a 16 bit system with 96 dB of dynamic range, was designed with 16 channels so that the field could be collected at two gain settings 40 dB apart.

Estimates of the vehicle trajectory during experiment x9814501 are illustrated in Fig. 3. The accuracy of the vehicle navigation was quite poor from an acoustic point of view. The inexact measurement of the pinger locations, the unknown sound speed field between the pingers and the AUV, the strong multipath arrival structure of the very shallow water environment and the state of the art in the AUV navigation filters together placed very coarse limits of ± 1 m on the vehicle location. In addition, significant biases were seen in the navigation for south traveling legs which implied unresolved problems with the navigation software [1]. Thus while the acoustic measurements made on the swordfish array were of generally good quality, with sufficient reverberation to noise ratio to image targets, the coherent combination of this data over successive TOPAS pings to create a synthetic aperture represents a very real challenge. In addition, the exact time the TOPAS transmissions occur in absolute time is unknown, due both to the fact that the vehicle acquisition system was unsynchronized to the TOPAS system, and to the fact that the standard deviation of the TOPAS firing time was approximately 10 ms. Thus the straightforward application of conventional monostatic synthetic aperture concepts was clearly not possible, and the problems of inaccurate vehicle position and unknown source trigger time and location need to be circumvented in order to demonstrate SAS concepts for this dataset.

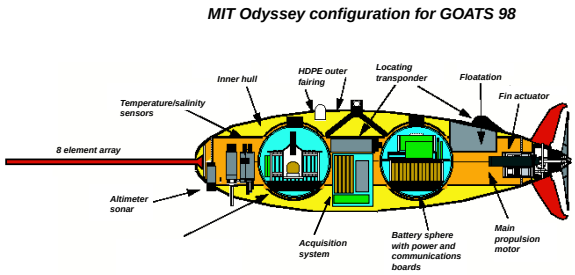

Fig. 2. A diagram of the MIT Odyssey AUV showing the 0.7 m long 8 element "swordfish" array deployed off the bow and the 50 kHz 16 channel dual gain acquisition system amidships.

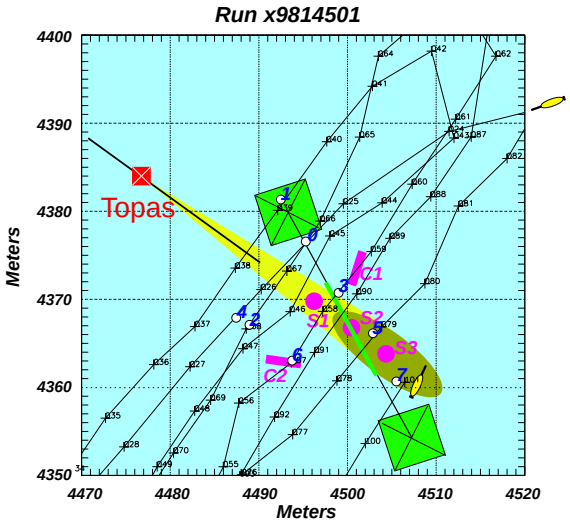

Fig. 3. The AUV trajectory during GOATS'98 experiment x9814501. Bistatic scattering from targets S2 and S3 is measured on the AUV as it swims back and forth over the target field. Data from file 25 is processed in this paper.

III. Experimental Results

A spectrogram of a typical dataset collected on the AUV nose array is illustrated in Fig. 4. The AUV acquisition

system begins recording after instructing the AUV navigation system to begin an LBL interrogation sequence. The clipped returns from the six LBL transponders operating at 500 Hz intervals between 8 and 10.5 kHz are seen at times between 0.3 and 0.6 s at the left of the spectrogram. The TOPAS detects the LBL interrogation cycle and after waiting 2 s for reverberation from the LBL cycle to die down begins sending 8 kHz Ricker pulses every 300 ms. These transmissions are clearly visible as the vertical stripes on the spectrogram. During these transmissions, the AUV is traveling at an average speed of approximately 1 m/s or 2 kts. The rate of the TOPAS transmissions, the vehicle velocity and the length of the swordfish array together determine that only roughly the front three of the eight elements of this array collect new information about the field scattered from the target area for each consecutive ping. The fact that there is significant array overlap between successive pings means that autofocusing concepts from traditional SAS [4], [5] may be used to help resolve difficulties associated with navigational uncertainty and trigger timing.

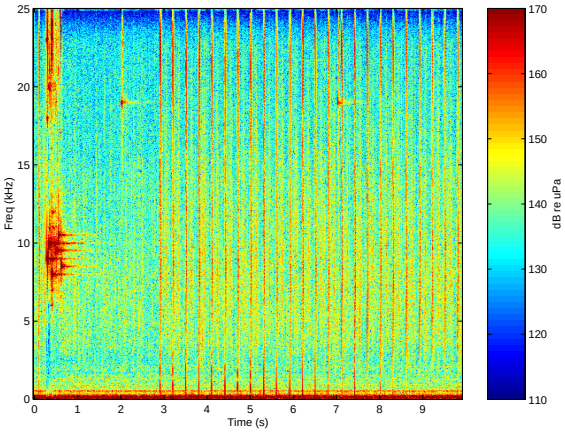

Fig. 4. Spectrogram of file 25 of the AUV data acquisition system from experiment x9814501 shows the LBL interrogation pings followed 2 s later by 24 TOPAS transmissions on the proud target S3 at 300 ms intervals.

Although as illustrated in Fig. 4 the TOPAS fires roughly every 300 ms, the trigger times are quite imprecisely known, with a standard deviation on the order of 10 ms due to the design of the TOPAS trigger. Thus when snippets of data are extracted and stacked, there is an evident lack of synchronization of the arrivals associated with the source and the various targets. For traditional monostatic MCM sonars, the returns scattered from the target field would be known in absolute time from the source trigger time, since the source trigger is readily available on a monostatic platform. For bistatic situations such as in the GOATS'98 dataset, the source trigger time and the total absolute travel time from the source to the target field and back is only approximately known. To give a better feel for the distinguishing characteristics of the data, 100 consecutive 65 ms snippets of the nose array time series containing the TOPAS direct and target scattered fields from files 23 through 27 have been extracted and aligned by hand. The

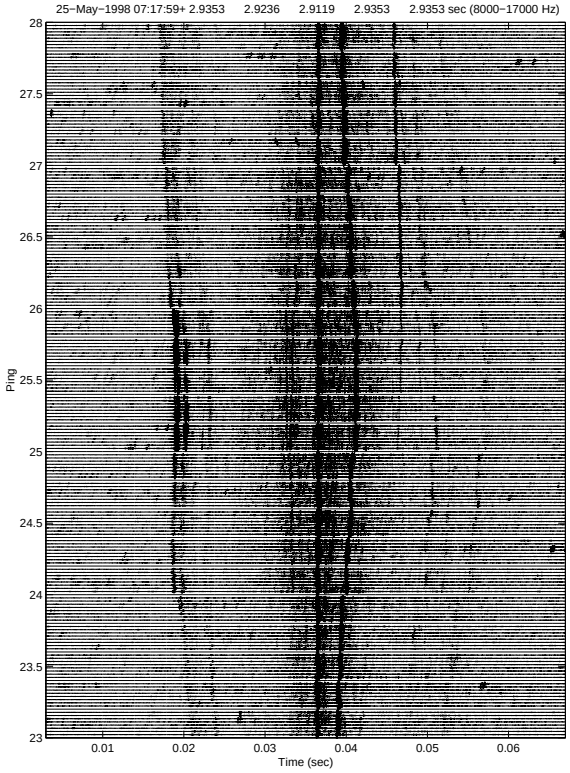

Fig. 5. The time series data from files 23 through 27 are shown in the 8-17 kHz band aligned by the time of arrival of the first scattered return from S3 (37 ms.) The first surface multiple of the S3 return is clearly visible at times between 39 and 41 ms. The direct TOPAS arrivals and the first surface and bottom multiples are visible at times between 17 and 23 ms. Two scattered returns from the flush buried sphere S2 are also faintly visible at a arbitrary time of approximately 35 ms.

result is shown in Fig. 5. The strongest return on which the data have been aligned turns out to be the direct scattered return from the flush buried sphere S3. Right behind this return is an almost equally strong surface multiple of the S3 return. Two further surface-bottom multiples are faintly visible to the far right at times between 47 and 57 ms. The fairly strong return seen for files 25-27 at a time of 46 ms is believed to be a scattered return from a fixed HLA deployed in a bistatic configuration over the target field during this period of the experiment [1]. The three fainter returns to the far left, arriving at arbitrary times between 17 and 25 ms, are the direct arrival and the first bottom and surface multiple from the TOPAS. The reason that the amplitude of the source arrivals is smaller than the scattered returns from S3 is because the AUV is out of the main transmission beam of the TOPAS.

The scattered returns from the flush buried sphere S2 are just visible in the data between the times of 32 and 35 ms. Unlike the return from the proud sphere S3, there are clearly two returns associated with the target itself. It is hypothesized that the first of these returns is caused by scattering from the part of the sphere closest to the sediment-water interface, and that the second return, which comes approximately 0.5 ms later, is the first membrane wave S_o multipath [6], [7]. The amplitude of these

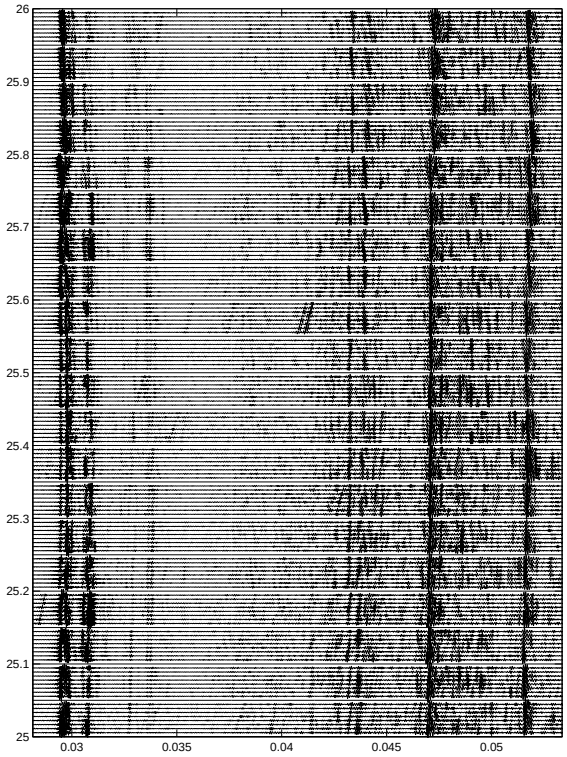

Fig. 6. Closeup of the bandpassed scattered field received on all eight elements of the nose array of the AUV for 20 TOPAS pings in file 25 of experiment x9814501. Here the large S3 arrival at 47 ms and the two S2 arrivals at 43.5 and 44 ms are clearly visible. Runout of the arrivals on the individual eight element arrays is minimal, indicating that the scatterers are observed near broadside during this file. Also clearly visible is the scattering from the rough sand in the ensonified footprint of the TOPAS, beginning around 37 ms.

two returns from S2 are significantly lower than those of the single strong return from S3, and are not too far above the reverberation background of the bottom patch ensonified along with S3. In Fig. 6 the 20 pings from file 25 are shown enlarged to better appreciate the details of the data. In this case the time series have been aligned along the axis of the first arrival. All eight time series from the nose array on the AUV are shown for each ping. The relative amplitude of the S2 and S3 returns may be appreciated from this figure. In addition, the increased reverberation from the ensonified patch may be observed in the individual time series to begin at the arbitrary time of roughly 37 ms.

In order to estimate the vehicle velocity a correlation log procedure [8] was applied to the part of the time series shown in Fig. 6 which was between the times of 37 and 46 ms. The results are illustrated in Fig. 7, where the peak cross correlation value between successive pings received on the physical aperture is shown averaged over the front four array elements of the n^{th} ping. It is seen that the average correlation lag between the n and $n+1$ pings is roughly 4 spatial elements (1 element corresponding to no motion), while between the n^{th} and $n+m$ pings it is $N(m-1)+1+(lag-1)m$ where $N=8$ is the number of elements in the physical aperture. For $m=2$, this gives a peak spatial correlation at 15 elements, which is also seen

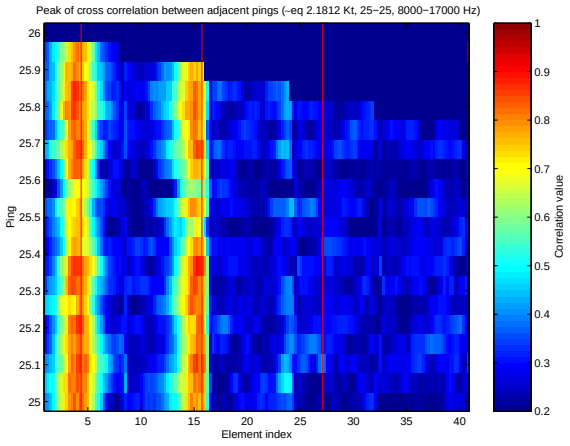

Fig. 7. The maximum inter-ping correlation coefficient vs physical element index. The far left corresponds to the correlation coefficient between the first element of physical aperture for the n and $n+1$ pings, corresponding to no array displacement. Instead the largest coefficient is seen between the first element of the n^{th} ping and the fourth element of the $n=1$ ping, corresponding to physical displacement of 3 elements between pings.

in Fig. 7. For m greater than 2, there is no correlation because the physical aperture no longer overlaps its previous position after two subsequent pings. The peak correlation (ρ^2) values themselves lie between 0.7 and 0.9, corresponding to reverberation to noise ratios (RNR) between roughly 4 and 10 dB. A correlation value of 0.5 corresponds to a RNR of 0 dB.

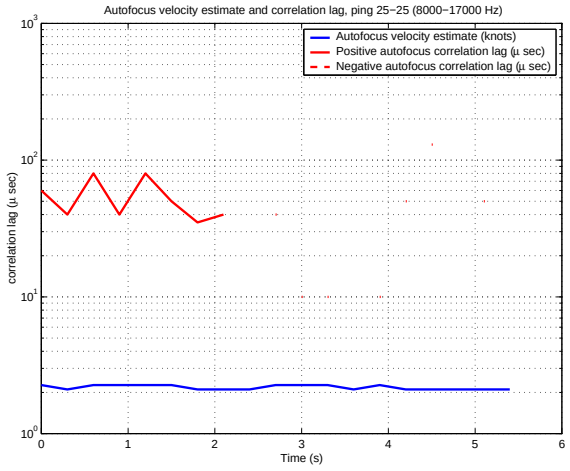

Fig. 8. The local velocity estimate from the interping correlation element lag (blue) and lag of the maximum interping correlation in time in μs (red). The estimated vehicle velocity corresponds to the known operating conditions of the AUV during file 25 of experiment x9814501.

In Fig. 8 the velocity estimate of the vehicle and the lag of the maximum correlation in μs are shown in a semilog format. The abscissa is the total time occupied by the 20 pings, and the ordinate is either the vehicle speed in knots (shown in blue), or the lag time (in red.) These results show that the average maximum correlation lag of 3 elements or $3 \times 0.1m/300ms \equiv 1$ m/s corresponds to vehicle speeds between 1.8 and 2.3 kts and that the maximum correlation

occurs at time less than 0.1 msec from times obtained by manual alignment of the time series to the direct TOPAS arrival as shown in Fig. 6.

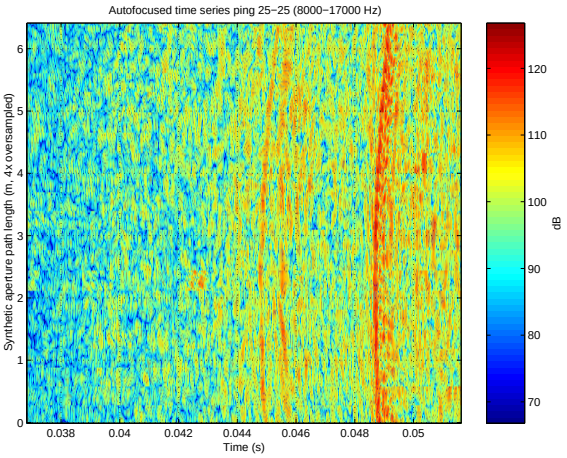

Fig. 9. The 6.3 m long synthetic aperture for file 25 constructed by appending physical apertures at the element lag of maximum correlation, shifting the time series by the associated temporal lag of the maximum spatial lag. The resulting synthetic aperture shows that scattering from both the proud sphere S3 (times after approximately 49 ms) and the flush buried sphere S2 (two returns between 44.5 and 45.5 ms arbitrary time) has been measured in the nearfield.

Under the assumption that the AUV follows a straight trajectory during a single 10 s duration acquisition cycle, it may be hypothesized that a useful synthetic aperture of the scattered field measured during a single acquisition cycle may be constructed by simply appending the successive pings at the spatial point of maximum correlation shifted in time by the appropriate correlation lag. The result of this process is illustrated in Fig. 9. Here the two arrivals from S2 and the first scattered return from S3 are both clearly visible. The size of the synthetic aperture is 6.3 m or roughly 9 times the length of the physical aperture of the array. The curvature of the S2 and S3 arrivals also clearly indicate that these target have been received in the nearfield of the synthetic aperture.

The hypothesis that the AUV trajectory is a straight line during the 10 s acquisition cycle can be tested by attempting to fit the hypothetical arrival times on a straight trajectory to the measured arrival times from a target of opportunity. In the case of experiment x9814501, the ensonification of S3 always provides a clear scatterer of opportunity. The results of the fit of the arrival times of S3 to a straight trajectory hypothesis are illustrated in Fig. 10. The straight trajectory runout fit is very good, and carries the added benefit that the standoff distance x from the AUV to the target (here $x = 8.8$ m assuming a background sound speed of $c_o = 1520$ m/s) is a byproduct of the fit procedure. The proximity of the scatterer to the AUV trajectory is determined by the curvature of the arrival structure at the point of closest approach. Under the hypothesis of straight travel, it is seen that the problem of the unsynchronized AUV data may be largely overcome, with the additional benefit that in the case of nearfield scatterers an estimate of the vehicle standoff distance may be

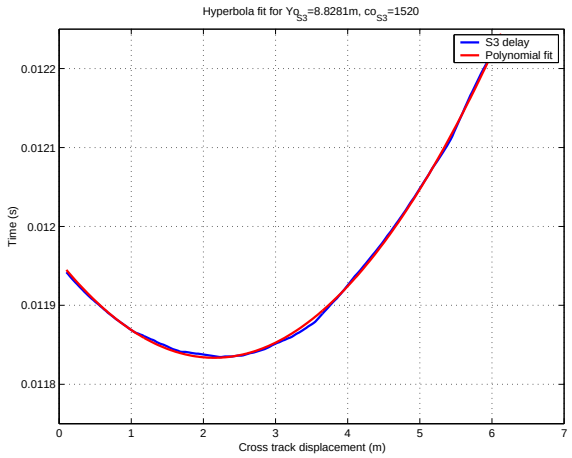

Fig. 10. The agreement between the arrival times of the scattered field from the proud sphere S3 and an analytic fit based on the assumption that the vehicle moves on a straight trajectory during file 25 of experiment x9814501. The best fit was obtained with a horizontal standoff range of 8.8 m assuming a background sound speed of $c_o = 1520$ m/s.

obtained and evaluated for consistency with navigational data obtained from the LBL network.

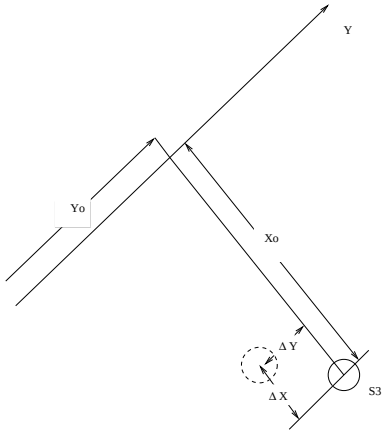

Fig. 11. The AUV trajectory notation used for determining nearfield beamforming parameters.

IV. Bistatic Synthetic Aperture Processing

The autofocused data shown in Fig. 9 may be processed coherently over the near-field synthetic aperture by a simple bistatic SAS algorithm. In arbitrary time coordinates, the time of arrival of the return from a point scatterer of opportunity (S3 in the processing described in this paper) from a bistatic source a distance R from this scatterer is (see Fig. 11)

$$T_{S3} = R/c_o + \sqrt{x_o^2 + (y - y_o)^2 + z_o^2}/c_o + T_o, \qquad (1)$$

where T_o is the arbitrary offset time, x_o is the horizontal point of closest approach of the linear AUV trajectory to S3, z_o is the height of the AUV above S3, and $y - y_o$ is the linear distance along the trajectory away from the point of

closest approach. Then if S2 is hypothesized to lie a distance $[\triangle x, \triangle y]$ away from S3 at the same value of Z (flat bottom hypothesis,) and the bistatic angle between the direction vector connecting the source to S3 and the vector connecting S3 to the point of closest approach on the AUV trajectory is θ, then under the assumption that the source is in the far field the arrival time from the hypothesized location of $S2$ is closely approximated by

$$T_{\widehat{S2}} = (R - (x_o - \triangle x))\cos\theta/c_o + \sqrt{(x_o - \triangle x)^2 + (y - y_o - \triangle y)^2 + z_o^2}/c_o + T_o. \quad (2)$$

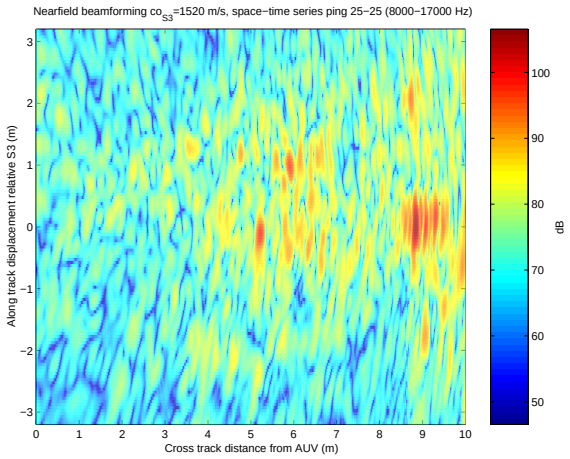

Fig. 12. The nearfield beamformed synthetic aperture for the 20 pings in file 25 of experiment x9814501. The proud sphere is clearly seen at an along track displacement of $y - y_o = 0$ m and the cross track displacement of $x_o = 8.8$ m. Two returns from the flush buried sphere S2 are seen at standoff ranges of approximately $\hat{x} = (x_o - \triangle x) = 5.25$ and 5.75 m, and along track displacements of $y - y_o = -0.2$ and 1.0. The second return is believed to be the first multipath of the S_o membrane wave of the sphere.

The result of summing all the autofocused time series at the times given in Eq. 2 for a range of hypothesized values of $[\triangle x, \triangle y]$ in the 8 to 17 kHz frequency band for file 25 from experiment x9814501 is illustrated in Fig. 12. Here it is seen that the detection on S3, at a standoff range of $x_o = 8.8$ m and an along track displacement relative to the point of closest approach of $\triangle y = 0$ m, has a spatial width of approximately 0.4 m, which is consistent with the theoretical resolution of a Hanning shaded 6.3 m long aperture at the estimated standoff range. Two detections of S2 are also found, at standoff ranges of approximately $\hat{x} = (x_o - \triangle x) = 5.25$ and 5.75 m, and along track displacements of $y - y_o - \triangle y = -0.2$ and 1.0. The second return is likely the first round trip of the S_o membrane wave of the target, which modeling studies have shown arrives with a time lag of approximately 0.5 ms. The fact that the beamforming finds an along track spatial shift for this arrival is likely due to the dispersive nature of this arrival [7]. Inspection of Figs. 5, 6 and 9 shows that the delay between the first and second S2 arrivals is indeed a fairly strong function of position along the AUV trajectory.

In Fig. 13 the hypothesized arrivals times of the first return from S2 and the S3 arrival are shown superimposed

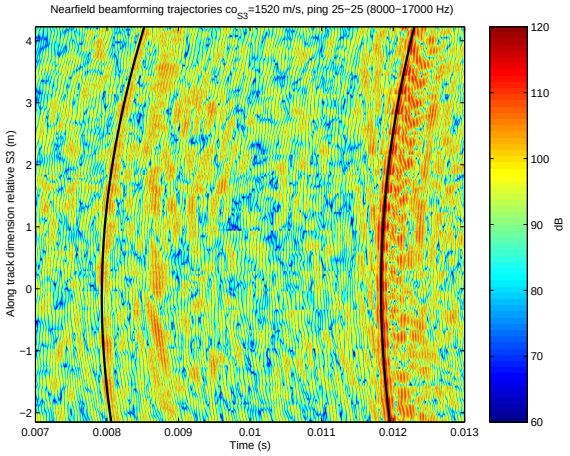

Fig. 13. Temporal trajectories corresponding to maximum returns from S2 (left curve) and S3 (right curve.) Close inspection of these trajectories show that the scattered field from these two targets is being coherently summed over the entire 6.3 m synthetic aperture constructed for file 25.

on the autofocused time series. Close inspection of the trajectories shows that they are fully coherent with the data over the entire synthetic aperture. The second S2 return is less obviously a fully coherent return over the entire synthetic aperture, consistent with modeling studies conducted at SACLANTCEN which have shown an interference structure in the sphere multipath associated with the S_o membrane and the A_{o-} antisymmetric wavetypes of the sphere [7].

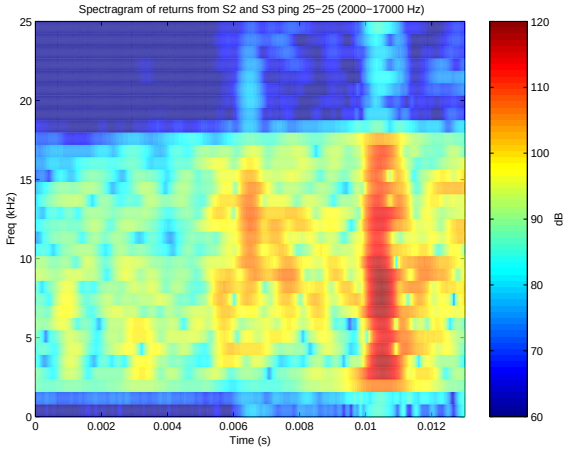

Fig. 14. The spectrogram of the beamformed time series for file 25 centered on the image of S2. Clearly visible is the time frequency response of the flush buried sphere between times of 6 and 8 ms. Below 8 kHz, S2 has one weak return at 6 ms, while in the 8-15 kHz range there are two distinct returns, the second of which is considered to be a membrane wave multipath of the sphere. The return from the proud sphere S3 is clearly visible at 10.5 ms. The source spectrum of the incident 8 kHz Ricker has not been deconvolved from this result.

The spectrogram of the nearfield beamformed data at the along track location of the first S2 return is illustrated in Fig. 14. The time-frequency response of S2 is found between the times of 6 and 8 ms and has a very interesting character. Between frequencies of 3 and 8 kHz a single return is seen at a time of 6 ms, while at higher frequencies

two returns are seen at 6.5 and 7.5 ms. It is hypothesized that the lower frequency response is associated with the geometric component of the evanescent excitation and scattering from the sphere, while the higher frequency response is associated with excitation by the evanescent lateral wave of membrane waves in the sphere at the sediment-water interface, with a subsequent return from the first resonance of the membrane wave S_o via the headwave path. However, without supporting modeling studies, these results remain open to interpretation.

A supercritical dataset from experiment x9814601 has also been analyzed to show how the returns from S2 change when it is ensonified at higher grazing angles. During this experiment the TOPAS source was moved forward to a position of 12.5 m along the rail, and the source was pointed at the S2 target. At this source position, the buried targets S1 and S2 are more strongly excited than in experiment x9814501 for three reasons, 1) because they are ensonified at higher grazing angles of 24.4° (S2) and 30.5° (S1) which are both above the critical angle, 2) because the source is focused on S2 instead of S3, so S1 is inside the ensonified patch, and 3) because the source is only 20 m from S1, so there is less TL than in experiment x9814501, where the source was 7.5 m further away. In addition, the scattered returns from the rough sandy bottom are much larger for the first and third reason. The result is that the RNR ratio increases from the 4 to 10 dB seen in experiment x9814501 for file 25 to values between 8 and 15 dB for file 47 in experiment x9814601.

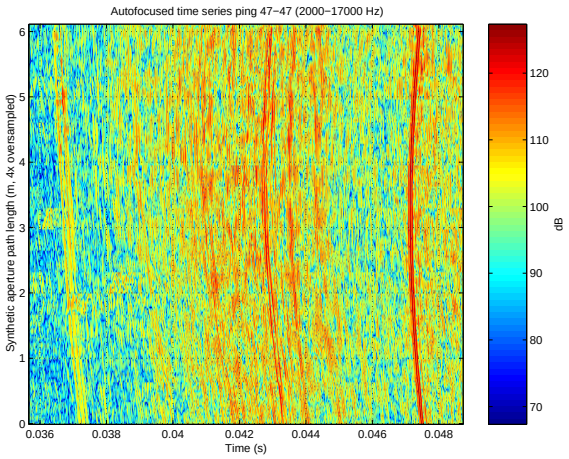

Fig. 15. The 6.1 m long synthetic aperture constructed for 18 pings from file 47 of experiment x98145601. Here the AUV is focused on S2 and the AUV passes almost directly over this target at a favorable bistatic angle. The return from S1 is faintly visible between 39 and 40 ms arbitrary time. The S2 returns are visible between 42 and 44 ms, and the S3 returns commence at about 47 ms.

In Fig. 15 the 6.1 m long autofocused synthetic aperture response for file 47 of experiment x9814601 is shown. The return from the proud sphere S3 is seen after times of 47 ms, while the scattered return from the rough sandy sediment-water interface is seen between times of 39 to 45 ms. Inside this scattering are buried the returns from S1 (between 39 and 40 ms) and S2 (between 43 and 44 ms.) The strong return to the far left between 36 and 37 ms is a source multiple.

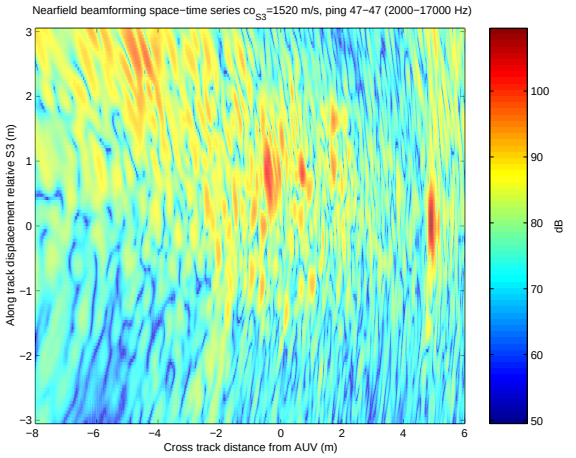

Fig. 16. The nearfield beamformed image of the target field for file 47 from experiment x9814601, where the TOPAS is directed towards S2 at a 24.4° grazing angle. The target of opportunity is at $y - y_o = 0$ m and $x_o = 4.9$ m. The first return from S2 is at $y - y_o = 0.8$ m and $x = -0.5$ m. The faint return from S1, ensonified above critical at a grazing angle of 30.5° is seen at $x = -5$ m and $y - y_o = 2.6$ m.

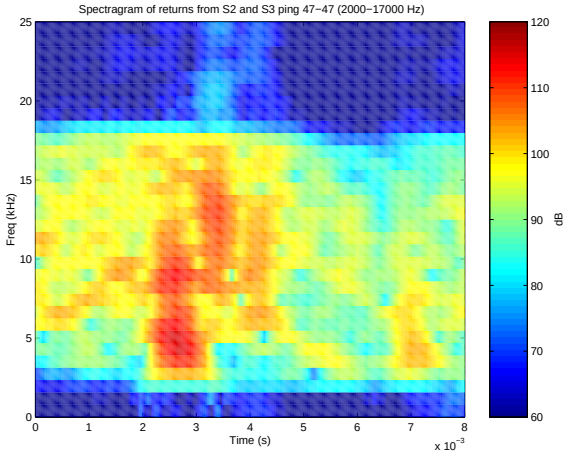

Fig. 17. The spectrogram of the beamformed time series from file 47 from experiment x9814601, where S2 is ensonified above critical at 24.4° clearly shows a stronger first arrival between 2 and 12 kHz at 2.5 ms, followed by the first multiple between 6 and 15 kHz at 3.25 ms.

The result of nearfield beamforming Fig. 15 are shown in Fig. 16. As opposed to file 25 from experiment x9814501, here the imaging results show that the AUV was not traversing perpendicular to the target field axis. The proud sphere S3 is imaged at $y - y_o = 0$ m, $x = 4.9$ m, the first return from S2 is imaged at $y - y_o = -0.5$ m, $x = 0.8$ m, and the return from the deep buried sphere S1 is visible at $y - y_o = 2.6$ m, $x = -5$ m. S1 and S2 are both clearly imaged in this case because they are both excited and observed above the critical angle. The spectral characteristics of these returns is also significantly changed by the more favorable geometry. The spectrogram of the return from S2 is shown in Fig. 17. Comparison with Fig. 14 shows that when the incident field is above critical, the frequency

content of the first arrival extends all the way to the low frequency cutoff of the analysis band, while the second and third returns associated with the elastic response of the sphere are less strongly affected by the angle of incidence.

V. Conclusions

Results from the GOATS'98 experiment indicate that bistatic synthetic apertures may be reliably generated by AUV's for the enhanced detection of objects buried in fast sediments and ensonified below the critical angle in the 2 to 20 kHz frequency range. Difficulties associated with inaccurate vehicle navigation and poor intra-vehicle communication can be largely overcome when the vehicle flies in a straight line and a target or pinger of opportunity is available to anchor the processing in space. In the results presented here, simple correlation autofocusing was combined with the availability of the proud target S3 to generate a nearfield time series and to beamform it as a function of cross and along track distance from the AUV trajectory to obtain images of buried objects.

Results show that when excited by an 8 kHz Ricker pulse below the critical angle of the sediment, the flush buried sphere S2 was most visible in the 8 to 15 kHz frequency band, with lower levels of backscatter in the 3 to 8 kHz band. These results conflict with the suggestion that subcritical detection of buried objects is best performed at the lowest possible frequencies, since the mechanism for target ensonification and subsequent rescattering is the evanescent wave, which exponentially decreases it's penetration at higher frequencies. Instead it is hypothesized that this unexpected high frequency response of S2 is associated with excitation and re-radiation of membrane waves in the part of the target closest to the seabed. Analysis of experiment x9815601 also shows that when S2 is ensonified above the critical angle, the low frequency response is enhanced. It is possible that in the experimental scenarios examined in this paper, where the AUV passes bistatically over the scatterers at above critical angle, the favorable reradiation of the scattered field into high angles makes the targets more visible in the higher frequency range of the 2 to 20 kHz band. Further processing of bistatic data collected both on the AUV and on the bistatic HLA deployed during this experiment, and further modeling studies are required to determine conclusively the mechanisms for the excitation and subsequent scattering from buried objects observed in bistatic geometries.

VI. Acknowledgments

The authors wish to acknowledge Joseph Edwards of MIT, and Edoardo Bovio and Reginald Hollett of SACLANTCEN for their assistance acquiring and processing the AUV data used in this paper. The MIT portion of this work was funded by ONR.

References

[1] H. Schmidt , A. Maguer, E. Bovio, W.L.J. Fox, K. LePage, N.G. Pace, R. Hollett, P. Guerrini, P.A. Sletner, E. Michelozzi, B. Moran and R. Grieve, "Generic Oceanographic Array Technologies (GOATS)'98 - Bistatic Seabed Scattering Measurements using Autonomous Underwater Vehicles," SR-302, SACLANT Undersea Research Centre, La Spezia, Italy (1998).

[2] A. Maguer, E. Bovio, W.L.J. Fox and H. Schmidt, "*In situ* estimation of sediment sound speed and critical angle," J. Acoust. Soc. Am. **108** 987-996 (2000).

[3] O. Bergem and N.G. Pace, "Calibration of the TOPAS PS040. Part I: Measurements recorded with the TOPAS acquisition system," SM-119, SACLANT Undersea Research Centre, La Spezia, Italy (1996).

[4] A. Bellettini, S. Fioravanti and M. Pinto, "Preliminary experimental investigation of synthetic aperture sonar micronavigation," SM-355, SACLANT Undersea Research Centre, La Spezia, Italy (1999).

[5] M.A. Pinto, S. Fioravanti and E. Bovio, "Accuracy of synthetic aperture sonar micronavigation using a displaced phase center antenna," SM-352, SACLANT Undersea Research Centre, La Spezia, Italy (1998).

[6] A. Tesei, A. Maguer, W.L.J. Fox and H. Schmidt, "Measurements of acoustic scattering from partially and completely buried spherical shells," SM-362, SACLANT Undersea Research Centre, La Spezia, Italy (1999).

[7] M.A. Pinto, A. Bellettini, R. Hollett and A. Tesei, "High resolution imaging of buried targets," submitted to special issue of IEEE J. of Ocean. Eng. on High Frequency Acoustics II (2001).

[8] P.N. Denbigh, "A design study for a correlation log to measure speed at sea," J. Navigation **35** 160-184 (1982).

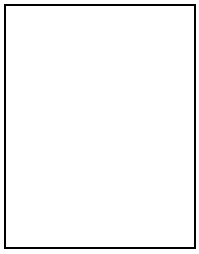

Kevin D. LePage was born in East Lansing, Michigan in 1961. He received his BS from Webb Institute in 1983, and his SM and PhD in Ocean Engineering from MIT in 1986 and 1992 respectively. From 1983 to 1987 he was a Naval Architect at DTNSRDC in Cabin John, MD where he developed conceptual designs for naval combatants. From 1992 to 1997 he was Scientist and later Senior Scientist at BBN, Cambridge, MA where he worked on problems related to propagation and scattering in the Arctic, hydroacoustic detection of nuclear detonations, active noise and vibration control and structural acoustics. Since 1997 he has been Senior Scientist at SACLANTCEN, where his primary responsibility has been the development of acoustic models for the prediction of scattering and reverberation in shallow and very shallow water at low to mid frequencies.

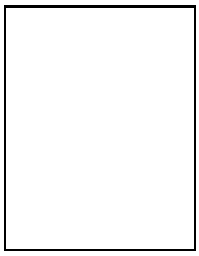

Henrik Schmidt was born in Denmark in 1950. He received his MS degree in Civil Engineering from the Technical University of Denmark in 1974, and his PhD. degree in Experimental Mechanics from the Technical University of Denmark in 1978. Holding positions of Research Fellow from 1978 to 1980 at the Technical University of Denmark, and from 1980 to 1982 at Risoe National Laboratory, Denmark, he worked on numerical modeling of wave propagation and scattering phenomena in relation to non-destructive testing of structures. From 1982 to 1987 he was Scientist and Senior Scientist at SACLANT Undersea Research Centre, Italy, where he developed the SAFARI code for modeling seismo-acoustic propagation in ocean waveguides. In 1987 he joined MIT where he is currently Professor and Associate Head of Ocean Engineering. His primary research interest is the interaction of underwater sound with seismic waves in the seabed and the Arctic ice cover. Other interests include computational acoustics and matched field processing, and the use of acoustics in autonomous oceanographic sampling networks. Prof. Schmidt is a fellow of the Acoustical Society of America, and a member of the Society of Exploration Geophysicists.